Nonperiodic metallic gratings transparent for broadband terahertz waves

Xiao-Ping Ren, Ren-Hao Fan, Ru-Wen Peng, Xian-Rong Huang, Di-Hu Xu, Yu Zhou, and Mu Wang

Phys. Rev. B **91**, 045111 — Published 12 January 2015

DOI: 10.1103/PhysRevB.91.045111

Non-periodic metallic gratings transparent for broadband terahertz waves

Xiao-Ping Ren,[1] Ren-Hao Fan,[1] Ru-Wen Peng,[1,*] Xian-Rong Huang,[2,*]
Di-Hu Xu,[1] Yu Zhou,[1] and Mu Wang[1]

[1] *National Laboratory of Solid State Microstructures and School of Physics, Collaborative Innovation Center of Advanced Microstructures, Nanjing University, Nanjing 210093, China*
[2] *Advanced Photon Source, Argonne National Laboratory, Argonne, Illinois 60439, USA*

Abstract

In this work, we demonstrate both theoretically and experimentally that non-periodic metallic gratings can become transparent for broadband terahertz waves. It is shown that broadband high transmission appears in aperiodic metallic gratings (including quasi-periodic and disordered ones), which originates from the non-resonant excitations in the grating system. Quasi-periodic and disordered metallic gratings effectively weaken and even eliminate Wood's anomalies, which are the diffraction-related characters of periodic gratings. Consequently, both the transparence bandwidth and transmission efficiency are significantly increased due to the structural aperiodicity. And an optimal condition is also achieved for broadband high transparency in aperiodic metallic gratings. Experimental measurements at terahertz regime reasonably agree with both analytical analysis and numerical simulations. Furthermore, we show that for a specific light source, for example, a line source, a corresponding non-periodic transparent grating can be also designed. We expect that our findings can be applied for transparent conducting panels, perfect white-beam polarizers, antireflective conducting solar cells, and beyond.

* To whom correspondence should be addressed. Electronic addresses: rwpeng@nju.edu.cn, xiahuang@aps.anl.gov

PACS: 42.25.Bs, 46.65.+g, 78.67.-n

I. Introduction

The interaction between light and matter, which leads to various interesting phenomena, is usually strongly dependent on the structural symmetry and the ordering degree in the natural or artificial materials. Based on the existence or lack of long-range and short-rang order, materials (or structures) may possess periodic, quasi-periodic and random ordering, respectively. Specifically, periodic structures have both long-range and short-range order; quasiperiodic structures bear long-range order but short-range disorder; random structures own neither long-range nor short-range order. It is well known that periodicity in structures brings about various important effects, such as what Bloch theorem illustrates, in solid state physics.[1] However, lack of periodicity may also create fascinating features on some occasions. For example, the extraordinary optical transmission (EOT) was initially discovered by Ebbesen and his coauthors[2] in periodic subwavelength hole array perforated on silver film, but later on, Matsui et al.[3] significantly presented enhanced transmission resonances of light through quasiperiodic arrays of subwavelength apertures and opened new avenues for optoelectronic devices.[4-10] Actually in the past decades, quite a few quasi-periodic structures,[11-13] such as structures with Cantor,[13] Fibonacci,[14-16] Thue-Morse,[17-19] and double-period sequences,[20,21] have received considerable attention.

It is known that broadband EOT is usually difficult to be achieved in the metallic/dielectric nanostructures. Fortunately by introducing self-similarity in the structures, people have successfully realized broadband EOT in quasiperiodic (such as Penrose-tiling) subwavelength metal/dielectric systems[3] and also in plasmonic fractals.[22] Physically, broadband EOT in these systems originates from resonant excitations of surface plasmons (SPs)[23] at multiple but discrete frequencies, which restrict the transparency bandwidth and transmission efficiency to some extents. Very recently, we have utilized periodic designing to successfully make structured metals transparent for broadband infrared and terahertz waves by relying on non-resonant excitation of spoof surface plasmons (SSPs) or SPs.[24-26] Similar phenomenon are further found in optical frequencies, which is explained by the anomalous impedance-matching mechanism.[27-30] However, the broadband transparence in periodic systems occurs for wavelengths larger than the first-order Wood's anomaly.[24,25] Around the Wood's anomalies,[31,32] the transmission of electromagnetic waves drops to zero because of the interference between the wavelets scattered by the periodic structures, which is essentially a diffraction effect of the periodic structures. To further broaden the transparency bandwidth and improve transmission efficiency of structured metals, we now try to exploit

aperiodic structures to break the transitional symmetry and decrease the degree of ordering in the system, then weaken or even eliminate Wood's anomalies, thus achieving broadband high transparency based on non-resonant excitations in aperiodic metallic gratings.

In this paper, we have theoretically and experimentally demonstrated that broadband high transmission appears in aperiodic metallic gratings (including quasi-periodic and disordered ones), which originates from the non-resonant excitations in the grating system. Quasi-periodic and disordered metallic gratings are capable to weaken and even eliminate Wood's anomalies, which consequently increase the transparence bandwidth and improve transmission efficiency in the terahertz (THz) region. Furthermore, with specially designed non-periodic metallic structure (a metallic grating with a gradually varying air void filling ratio, for example), the system can become transparent for transverse-magnetic (TM) polarized line sources. The broadband transparence for structured metals may have numerous important applications such as conducting panels,[7,33-35] white-beam polarizers,[36] anti-reflective solar cells,[27,37] etc.

The paper is organized as follows. After the introduction, in Sec. II, we theoretically investigate the broadband transparence in non-periodic metallic gratings based on detailed analytical solutions of Maxwell's equations. The optimal incident angle for broadband transparency of metallic gratings is achieved. In Sec. III, by using the finite-difference time-domain (FDTD) method, we present the numerical calculations on the optical transmission through periodic, Fibonacci and disordered metallic gratings, respectively. And electrical field distributions prove that broadband transparency in the metallic gratings originate from non-resonant effect. In Sec. IV, we show experimental results for the broadband transparence of non-periodic metallic gratings. Furthermore, in Sec. V, a metallic grating with a gradually varying air void filling ratio is demonstrated to be transparent for line sources. Finally, we summarize our results in Sec. VI.

II. Analytical analysis on broadband transparence in non-periodic metallic gratings

We consider electromagnetic waves traveling through a non-periodic metallic grating based on Maxwell's equations. Without loss of generality, we suppose that the non-periodic metallic grating is constructed by arranging units A and B according to a non-periodic sequence, such as the Fibonacci sequence or a disordered sequence, etc. As shown in Fig.1(a), Unit A has the overall unit size p_A, metal strip width b_A, and thickness h; the corresponding

parameters for Unit *B* are p_B, b_B, and thickness h, respectively. When transverse-magnetic (TM) polarized waves are incident on the sample, we can divide the space adjacent to the sample into three regions: the incident region (*I*) above the sample, the sample region (*II*), and the emitting region (*III*) below the sample. To simplify the analysis, we defined the vertical positions of the top and bottom grating surfaces as $z = 0$ and $z = h$, respectively. We consider the regions *I* ($z < 0$) and *III* ($z >$ h) as free space of air, and the metal is treated as an ideal metal. It follows that the *y*- component of magnetic field in regions *I* and *III* can be expressed as:

$$\begin{cases} H_y^I = \exp(ik_{x0}x + ik_{z0}z) + \sum_m r_m \exp(ik_{xm}x - ik_{zm}z) \\ H_y^{III} = \sum_m t_m \exp(ik_{xm}x + ik_{zm}z) \end{cases}, \tag{1}$$

where $k_{xm} = k_{x0} - \Delta k_{xm}$, Δk_{xm} is provided via high-order diffractive modes, $k_{zm} = (k_0^2 - k_{xm}^2)^{1/2}$, $k_{x0} = k_0 \sin\theta$, $k_0 = 2\pi / \lambda$, r_m and t_m are the *m*th reflection coefficient and transmission coefficient, respectively. When the wavelength is much larger than the sizes of the constituent units, high-order diffractive modes are evanescent and are neglected for simplicity. Thus, Equation (1) is simplified as:

$$\begin{cases} H_y^I = \exp(ik_{x0}x + ik_{z0}z) + r_0 \exp(ik_{x0}x - ik_{z0}z) \\ H_y^{III} = t_0 \exp(ik_{x0}x + ik_{z0}z) \end{cases}, \tag{2}$$

with $k_{z0} = (k_0^2 - k_{x0}^2)^{1/2} = k_0 \cos\theta$, $k_{x0} = k_0 \sin\theta$, $k_0 = 2\pi / \lambda$.

In region *II*, since the metal can be taken as ideal metal in present THz regime, the magnetic field is zero except in the slits ($p_n < x < p_n + a_n$), where p_n represents the corresponding starting coordinate of the *n*th slit, and a_n represents its width. The magnetic field in the *n*th slit ($p_n < x < p_n + a_n$) can be simply expressed as the zeroth-order rectangular waveguide mode:

$$H_{ny}^{II} = \cos[q(x - p_n)][M_n \exp(i\beta_s z) + N_n \exp(-i\beta_s z)], \tag{3}$$

where β_s is the wave number in the slits, q is eigen wave vector of waveguide, M_n and N_n are component coefficients, respectively. The relation between the *x*-component of the electric vector and the *y*-component of the magnetic vector is given as:

$$E_x = -\frac{i}{\omega\varepsilon}\frac{\partial H_y}{\partial z}. \tag{4}$$

The boundary conditions of the electric fields at the two grating surfaces should be satisfied, *i.e.*,

$$\begin{cases} \int_{-\frac{D}{2}}^{\frac{D}{2}} E_x^I \mid_{z=0} dx = \sum \int_{p_j}^{p_j+a_j} E_{jx}^{II} \mid_{z=0} dx \\ \sum \int_{p_j}^{p_j+a_j} E_{jx}^{II} \mid_{z=h} dx = \int_{-\frac{D}{2}}^{\frac{D}{2}} E_x^{III} \mid_{z=h} dx \end{cases}. \tag{5}$$

Meanwhile, the boundary conditions of the magnetic fields follow the relation

$$\begin{cases} \frac{1}{D} \int_{-\frac{D}{2}}^{\frac{D}{2}} H_y^I \mid_{z=0} dx = \frac{1}{W} \sum \int_{p_j}^{p_j+a_j} H_{jy}^{II} \mid_{z=0} dx \\ \frac{1}{W} \sum \int_{p_j}^{p_j+a_j} H_{jy}^{II} \mid_{z=h} dx = \frac{1}{D} \int_{-\frac{D}{2}}^{\frac{D}{2}} H_y^{III} \mid_{z=h} dx \end{cases}, \tag{6}$$

where $W = \sum a_j$ represents the sum of the width of all slits, and D is the total width of the sample, respectively.

By solving Eqs. (5) and (6), we can derive the reflection coefficient as:

$$r_0 = \frac{(k_{z0}^2 D^2 / W^2 - \beta_s^2) \tan(\beta_s h)}{(k_{z0}^2 D^2 / W^2 + \beta_s^2) \tan(\beta_s h) + 2i\beta_s k_{z0} D / W}. \tag{7}$$

Equation (7) indicates that if

$$k_{z0}^2 D^2 / W^2 - \beta_s^2 = 0, \tag{8}$$

the reflection coefficient reaches its minimum value $r_0 = 0$. When the slit is vacuum, we have $\beta_s = k_0$. Therefore, once Eq. (8) is satisfied, zero reflection and high transmission are achieved. Furthermore, the optimal incident angle for high transmission follows

$$\theta_f = \arccos(W / D). \tag{9}$$

Note that Equation (9) for non-periodic gratings looks like the expression for periodic gratings[24,25], but here in Eq. (9), air void filling ratio W / D is an average quantity representing the proportion of the empty space with respect to the volume of the entire non-periodic grating.

The above analysis indicates that broadband extraordinary transmission is an universal property of 1D metallic gratings under oblique incidence. The broadband transparence in aperiodic metal grating is not sensitive to the structural details of the grating when the incident wavelength is much larger than the sizes of the constituent units. Instead, it is primarily dominated by the averaged structural geometry, such as air void filling ratio.

III. Numerical simulations on broadband transparence in metallic gratings

Based on the finite-difference time-domain (FDTD) method,[38] we have carried out the numerical calculations on the optical transmission through several metallic gratings with

periodic, Fibonacci and disordered sequence, respectively. All these metallic gratings are constructed by units *A* and *B*. In the calculations, Unit *A* has unit size p_A = 300 μm, metal strip width b_A = 210 μm and thickness h = 200 μm; while the corresponding parameters for Unit *B* are p_B = 500 μm, b_B = 350 μm, and h = 200 μm, respectively. The numerical calculations are implemented based on FDTD method with commercial software package Lumerical FDTD Solution 8.0.1. Metals in the THz region can be considered to be perfect electric conductors (PEC), and we set the relative permittivity of the metal to -1 and the conductivity to 1.6×10^7 $(\Omega m)^{-1}$ in the subsequent calculations, where $\sigma / (\varepsilon_0 \varepsilon \omega) >> 1$ is satisfied for a good electric conductor (here σ and ε stand for the conductivity and the relative dielectric permittivity of the metal, respectively.).

For the periodic metallic grating (S1) constructed by repeating Unit *A,* when the incident angle is θ = 0°, the high transmission peak (Fig. 1(b)) is caused by Fabry-Perot (FP) resonance occurring at $\lambda = 2h / N + \Delta_N$, where N > 0 is an integer and Δ_N is the redshift of the peak.[39-41] And, broadband high transmission caused by non-resonance effect occurs around the optimal incident angle of θ_f = 68° when the wavelength λ is larger than the first-order Wood's anomaly of $\lambda_{WD1} = p_A (1 + \sin\theta)$, as shown in Fig. 1(c). Meanwhile for the periodic grating (S2) constructed by repeating Unit *B*, similar FP resonance can be found at normal incidence (Fig. 1(d)), but FP resonance peak is partially truncated by the Wood's anomalies. At oblique incidence, as shown in Figs. 1(c) and 1(e), both periodic gratings (S1 and S2) have the same optimal incident angle of θ_f = 68° because they have the same ratio $(p_i - b_i) / p_i$ = 30% (i = *A*, *B*).[24,28] Note that in the short wavelength range, Wood's anomalies appear due to the diffraction effects, which sharply interrupt the continuous high transmission spectra. Therefore, broadband transparence in the periodic metallic grating occurs only for wavelengths larger than the first-order Wood's anomaly. However, this situation will be significantly changed for non-periodic metallic gratings as following.

The Fibonacci metallic grating (S3) constructed by units *A* and *B* is produced by repeating the substitution rules[11-13] $A \rightarrow AB$ and $B \rightarrow A$. We keep the air void filling ratio at $(p_{A(B)} - b_{A(B)}) / p_{A(B)}$ = 30% for each unit. Here our Fibonacci structure (S3) contains 89 units. When the TM-polarized waves go through the Fibonacci grating at normal incidence, as shown in Fig. 1(f), the wavelength of high transmission caused by FP resonance occurs around the similar one as the periodic gratings (Figs. 1(b) and 1(d)) because these gratings here have the same thickness, and the FP resonance peaks are mainly determined by the sample thickness. However, at oblique incidence, it is shown that the broadband high

transmission caused by non-resonant excitations, which we will demonstrate later, still occurs around the optimal incident angle of θ_f = 68° as shown in Fig. 1(g). We can see that the Wood's anomalies in Fig. 1(g) are significantly weakened by the structure changing from periodic to Fibonacci sequence. Note that the first-order Wood's anomalies move to the wavelength $\lambda_{Fib} = p_F\,(1 + \sin\theta)$, where $p_F = (\tau\, p_A + p_B) / (1+ \tau)$ with the golden ratio $\tau = (\sqrt{5} + 1) / 2$. Obviously λ_{Fib} is between the first-order Wood's anomalies $\lambda_{WD1} = p_A(1+\sin\theta)$ and $\lambda_{WD2} = p_B(1+\sin\theta)$ of the periodic gratings in Fig. 1(g). For the incident waves with $\lambda > \lambda_{Fib}$, we can achieve broadband high transmission at an optimal incident angle θ_f. Therefore, quasiperiodicity in the Fibonacci structure has significantly suppressed Wood's anomalies yet effectively kept non-resonant excitations that we will discuss later, which eventually lead to broadband high transmission in the Fibonacci metallic grating.

Meanwhile, the disordered grating (S4) contains two basic units *A* and *B* just the same as Fibonacci grating but with a disordered sequence, where Unit *A* and Unit *B* are arranged randomly. Here our disordered structure (S4) contains totally 100 units. Figures 1(h) and 1(i) are the calculated transmission spectra of TM waves in disordered metallic grating at incidence angles of θ = 0° and θ = 68°, respectively. At normal incidence, the wavelength of high transmission caused by FP resonance occurs because the grating have the same thickness as those we mentioned above. While at oblique incidence of θ_f = 68°, it is clearly shown that the broadband high transmission caused by non-resonance effect exists as shown in Fig. 1(i). Different from the periodic and Fibonacci gratings, the Wood's anomalies disappear in this disordered metallic grating. It indicates that the randomness in the structure has completely broken both long-range and short-range ordering, and manifested broadband high transmission of the TM-polarized waves in an extremely wide waveband.

It is interesting to discuss the dependence of the optimal incident angle on air void filling ratio *W* / D. As shown in Fig. 2, we illustrate the optimal incident angle as a function of air void filling ratio *W* / D in a series of disordered gratings, which are obtained by Eq. (9) and FDTD simulations, respectively. In each grating sample, we randomly generate the width of all the slits and strips but fix air void filling ratio, totally have for about 4cm-long sample with 100 metal strips. These two sets of results match well as shown in Fig. 2, particularly in the range with small *W* / *D*. As *W* / *D* becomes larger, the electromagnetic field in the slits cannot be simply expressed as the zeroth-order rectangular waveguide mode, instead, the high-order modes should be included in the analytical analysis. The high-order modes may reduce the wave number of the THz waves propagating through the slits, and then influence

the overall the reflection coefficient, which leads to larger θ_f predicted by Eq. (9) compared to FDTD simulations.

For further understanding the physical mechanisms of the broadband high transmission, we have calculated the electric field distributions in periodic and non-periodic gratings at the high transmission wavelengths for both normal incidence and optimal angle incidence (as shown in Fig.3). For normal incidence, all the electric field ($|\mathbf{E}|^2$) distributions are very similar in periodic gratings (Figs. 3(a) and 3(c)), Fibonacci grating (Fig. 3(e)), and disordered grating (Fig. 3(g)). And we can find high $|\mathbf{E}|^2$ distribution at every corner of the strip, which means high transmission comes from resonant excitations, so they belong to narrowband effects. However, for optimal incidence at $\theta_f = 68°$, all the $|\mathbf{E}|^2$ distributions in periodic gratings (Figs. 3(b) and 3(d)), Fibonacci grating (Fig. 3(f)), and disordered grating (Fig. 3(h)) show that no obvious enhancement of electric fields at two neighboring corners, thus the resonances do not happen in these systems. These evidences indicate that the broadband high transmission is indeed caused by non-resonance effect in the metallic grating systems.

IV. Experiments of the broadband high transmission in metallic gratings

The above broadband high transmission in metallic gratings can be further experimentally demonstrated. In the experiments, we fabricated four types of gratings containing two periodic gratings (S1 and S2) and two non-periodic gratings (S3 and S4) just as discussion in Sec. III. During the fabrication process, the grating pattern was first designed via software (AutoCAD, 2007) and printed on both sides of a stainless steel plate via photochemical reaction. In order to construct the gratings, the uncoated parts of the stainless steel surfaces were then etched by chemicals on both sides. To protect the stainless steel grating and enhance the conductivity, all surfaces, including the slit walls, were coated with a nearly 3-μm-thick gold film by magnetron sputtering. The transmission spectra were measured by a THz real-time spectrometer (EKSPLA/THz, Lithuania). By scanning the delay line, we obtained the time-domain signal $E(t)$ of the polychromatic THz pulse transmitted through the samples. Thereafter, the transmission spectrum was obtained from the Fourier transform of $E(t)$ within the 0.3 – 1.5 THz frequency range and normalized with respect to the transmission spectrum of air.

Figures 4 and 5 show the sample photographs and measured transmission spectra of four different metallic gratings, respectively. In the transmission spectra of four gratings at normal incidence, we can find FP resonance peaks occur around the same wavelength because

grating samples here have the same thickness. Specially, the FP resonance peak is partially truncated by the Wood's anomaly in periodic gratings (as shown in Figs. 5(a) and 5(c)); but in non-periodic gratings (to see Figs. 5(e) and 5(g)), they become much weaker, which means that the Wood's anomalies in non-periodic gratings are not obvious.

While for optimal incident angle θ_f = 68°, the periodic gratings have high transmission for long wavelength larger than that for the Wood's anomalies, which is clear with very deep valley. For the grating S1 (as shown in Fig. 5(b)), the Wood's anomaly is at λ = 575 μm where the transmittance is less than 30% and the width of valley band is more than 80 μm. For the grating S2 (as shown in Fig. 5(d)), the Wood's anomaly is at λ = 950 μm where the transmittance is 27% and the band width of valley is more than 200 μm. So for further broadening the bandwidth of high transmission, we are restricted by the Wood's anomalies in periodic gratings. However, once we break the periodic order, different results are presented in Fig. 5(f) (Fibonacci grating) and Fig. 5(h) (disordered grating). Two little valleys in the measured transmission spectra for Fibonacci grating (S3) at λ = 530 μm and λ = 735 μm and none for disordered grating (S4) when at the optimal incident angle of θ_f = 68°. The transmittance of the non-periodic gratings remains very high, for wavelength from 875 μm to 945 μm in Fibonacci case, for wavelength from 965 μm to 1000 μm and wavelength larger than 1430 μm in disordered case, their transmittance is more than 90% which is much higher than for periodic gratings.

From above experimental measurements, we have demonstrated that metallic gratings can become transparent for extremely broadband THz waves under optical oblique incidence, which is found in periodic, quasi-periodic, and disordered gratings. The transparent bandwidth is broadened and transmission efficiency are improved in quasi-periodic and disordered systems due to the fact that Wood's anomalies are weakened or eliminated by non-periodicity. In order to evaluate the feature of band high transmission in the grating, we define a broadband high transmission factor as $\Delta = \frac{1}{\sigma}\cdot\frac{1}{\delta}$, where $\sigma = \sqrt{\int_{\lambda_{\min}}^{\lambda_{\max}} (T-\bar{T})^2/(\lambda_{\max}-\lambda_{\min})d\lambda}$ is the standard deviation which reflects the discrete degree of transmission compared with the mean value $\bar{T}$, and the quantity $\delta = \int_{\lambda_{\min}}^{\lambda_{\max}} [(1-T)/T]^2/(\lambda_{\max}-\lambda_{\min})d\lambda$ describes the transmission deviation compared with perfect transmission. Obviously, higher factor Δ indicates a band-broader and higher transmission. Based on experimental data shown in Fig. 5, we find that at the optimal

incident angle $\theta_f = 68°$, $\Delta_{Fib} \cong 34.7$ in Fibonacci grating S3, and $\Delta_{dis} \cong 25.5$ in disordered grating S4, which are much larger than those in periodic gratings as $\Delta_A \cong 18.6$ in S1 and $\Delta_B \cong 2.9$ in S2. All these experimental factors reasonable agree with the calculated ones (Note: $\Delta_A \cong 10.6$, $\Delta_B \cong 4.8$, $\Delta_{Fib} \cong 22.9$, and $\Delta_{dis} \cong 21.0$ from the data in Fig. 1). Therefore, compared with periodic cases, both Fibonacci and disordered gratings achieve much better feature on broadband high transmission.

Actually we can prove the phenomena on broadband high transmission more clearly in the angular transmission spectra for a metallic grating with the tenth-generation Fibonacci and disordered sequence given in Fig. 6. It is obvious that the Wood's anomalies are weakened but still exist for Fibonacci grating (Figs. 6(a) and 6(b)), but they nearly disappear for the disordered metallic grating (Figs. 6(c) and 6(d)) because of long-range disorder. Here, we have successfully broadened the high transmission band by making the units of the gratings disordered, so as to achieve maximum breaking of the Wood's anomalies which affect the bandwidth. Further studies can be carried on to find a unique aperiodic metallic structure with maximum feature of band high transmission by optimizing both the geometry of units and the ordering degree of the structure.

V. Design a specific structured metallic grating transparent for a line source

It is known that the THz waves, which cover the frequencies from 10^{11} to 10^{13} Hz, can bridge the gap between the infrared and the microwaves in the electromagnetic spectrum. The THz technology[42-44] has been applied in information and communications, imaging and sensing, biology and medical sciences, homeland security, and so on. In order to contribute to these applications, one of the key points is to manipulate the transmission of THz waves efficiently and actively. In recent years many novel electromagnetic phenomena have been found in terahertz region[45-47], such as extraordinary optical transmission (EOT) through structured metallic films and electromagnetically induced transparency (EIT) using metamaterial. Most of those studies have focused on the plane waves, however, in practical applications we may have different kinds of light sources, such as point sources and line sources. Our following simulations show that extraordinary transmission of light from a line source is also insensitive to the grating periodicity, which makes it possible to design specific structured metallic gratings to achieve broadband transparence for specific light sources.

As an example, we design a metallic grating with a gradually variation of air void filling ratio to achieve transparency of TM-polarized light from a line source along the Y-axis. As illustrated in Fig. 7(a), the structure consists of a large number of units, which have the identical width p along the X-axis. If we define the unit exactly below the line source as the zeroth order, the air void filling ratio of the nth unit is determined by the local incident angle φ according to $t_n = \cos\varphi_n = d_0 / (d_0^2 + n^2p^2)^{1/2}$, where d_0 is the distance between the line source and the grating. When the incident angle φ increases, the ratio t_n decreases. Therefore, this structure, which is specifically designed for a line source, has a gradually varying air void filling ratio. Figure 7(b) shows the simulated transmission spectra for several kinds of metallic gratings using TM-polarized line sources. In our simulation, the grating has the following parameters: p = 0.4 mm, d_0 = 2mm, width of 3.2 cm, and thickness of 0.2 mm. The transmission here is normalized to the intensity collected by the monitor in air. Obviously, our designed metallic grating (black line in Fig. 7(b)) can achieve more than 90% transmission for a line source. Interestingly, this high transmission is comparable to the results of the periodic grating for plane waves. In comparison, periodic gratings have much lower transmission for line sources. For example, the periodic grating with a constant ratio of air area of 30% has a transmission value of about 40% (red curve in Fig. 7(b)) under the incidence of a line source with d_0 = 2mm, and the periodic grating with a 40% air void filling ratio has around 60% maximum transmission (blue curve in Fig. 7(b)) even for long wavelengths. These results suggest that it is possible to make structured metallic gratings transparent for various kinds of light sources following the mechanism discussed in Sec. II.

VI. Summary

We have theoretically and experimentally demonstrated broadband high transmission of THz waves in quasi-periodic and disordered metallic gratings, which originates from the non-resonant excitations in the grating system. Quasi-periodic and disordered metallic gratings effectively weaken and even eliminate Wood's anomalies. Consequently, both the transparence bandwidth and transmission efficiency are significantly increased due to the structural aperiodicity. We also derive an optimal condition is also achieved for broadband high transparency in aperiodic metallic gratings. Experimental measurements at terahertz regime reasonably agree with both analytical analysis and numerical simulations. Furthermore, we show that for a specific light source, for example, a line source, a corresponding non-periodic transparent grating can be also designed. We expect that these

results would be of potential applications in many fields such as transparent conducting panels and stealth objects. In addition, the observed phenomena may also shed new light on the development of broadband metamaterials, including sonic artificial materials.

Acknowledgments

This work was supported by the Ministry of Science and Technology of China (Grant No. 2012CB921502), the National Science Foundation of China (Grants No. 11034005, 61475070 , 11474157, 11321063, and 91321312), and the China Postdoctoral Science Foundation (Grant No. 2014M551548). XRH was supported by the U.S. Department of Energy, Office of Science, Office of Basic Energy Sciences, under Contract No.DE-AC02-06CH11357.

REFERENCES:

[1]C. Kittle, *Introduction to Solid State Physics*. (John Wiley & Sons, New York,1996).

[2]T. W. Ebbesen, H. J. Lezec, H. F. Ghaemi, T. Thio, and P. A. Wolff, Nature (London) **391**, 667 (1998).

[3]T. Matsui, A. Agrawal, A. Nahata, and Z. V. Vardeny, Nature (London) **446**, 517 (2007).

[4]J. A. Porto, F. J. García-Vidal, and J. B. Pendry, Phys. Rev. Lett. **83**, 2845 (1999).

[5]H. Liu, and P. Lalanne, Nature (London) **452**, 728 (2008).

[6]Y. J. Bao, R. W. Peng, D. J. Shu, Mu Wang, X. Lu, J. Shao, W. Lu, and N. B. Ming, Phys. Rev. Lett. **101**, 087401 (2008).

[7]Z. Y. Song, Q. He, S. Y. Xiao, and L. Zhou, Appl. Phys. Lett. **101**, 181110 (2012).

[8]S. Zhang, D. A. Genov, Y. Wang, M. Liu, and X. Zhang, Phys. Rev. Lett. **101**, 047401 (2008).

[9]N. Liu, L. Langguth, T. Weiss, J. Kästel, M. Fleischhauer, T. Pfau, and H. Giessen, Nat. Mater. **8**, 758 (2009).

[10]L. Qin, K. Zhang, R. W. Peng, X. Xiong, W. Zhang, X. R. Huang, and Mu Wang, Phys. Rev. B **87**, 125136 (2013).

[11]B. B. Mandelbrot, *The Fractal Geometry of Nature*. (Freeman, New York, 1982).

[12]E. L. Albuquerque, and M. G. Cottam, Phys. Rep. **376**, 225 (2003).

[13]E. Maciá, Rep. Prog. Phys. **75**, 036502 (2012).

[14]R. Merlin, K. Bajema, R. Clarke, F. -Y. Juang, and P. K. Bhattacharya, Phys. Rev. Lett. **55**, 1768 (1985).

[15]R. W. Peng, A. Hu, S. S. Jiang, C. S. Zhang, and D. Feng, Phys. Rev. B **46**, 7816 (1992).

[16]W. Gellermann, M. Kohmoto, B. Sutherland, and P. C. Taylor, Phys. Rev. Lett. **72**, 633 (1994).

[17]A. Thue, Norske Vidensk. Selsk. Skr. I. Mat. Nat. Kl. Christiania **7**, 1 (1906).

[18]M. Morse, Trans. Am. Math. Soc. **22**, 84 (1921).

[19]Q. Hu, J. Z. Zhao, R. W. Peng, F. Gao, R. L. Zhang, and Mu Wang, Appl. Phys. Lett. **96**, 161101 (2010).

[20]J. M. Luck, Phys. Rev. B **39**, 5834 (1989).

[21]G. Steinmeyer, D. Jaspert, and F. Mitschke, Opt. Commun. **104**, 379 (1994).

[22]Y. J. Bao, H. M. Li, X. C. Chen, R. W. Peng, Mu Wang, X. Lu, J. Shao, and N. B. Ming, Appl. Phys. Lett. **92**, 151902 (2008).

[23]W. L. Barnes, A. Dereux, and T. W. Ebbesen, Nature (London) **424**, 824 (2003).

[24]X. R. Huang, R. W. Peng, and R. H. Fan, Phys. Rev. Lett. **105**, 243901 (2010).

[25]R. H. Fan, R. W. Peng, X. R. Huang, J. Li, Y. Liu, Q. Hu, Mu Wang, and X. Zhang, Adv. Mater. **24**, 1980 (2012).

[26]R. H. Fan, J. Li, R. W. Peng, X. R. Huang, D. X. Qi, D. H. Xu, X. P. Ren, and Mu Wang, Appl. Phys. Lett. **102**, 171904 (2013); C. Meng, R. W. Peng, R. H. Fan, X. R. Huang, and Mu Wang, Science China Information Sciences **56**, 120404 (2013).

[27]A. Alù, G. D'Aguanno, N. Mattiucci, and M. J. Bloemer, Phys. Rev. Lett. **106**, 123902 (2011).

[28]N. Aközbek, N. Mattiucci, D. de Ceglia, R. Trimm, A. Alù, G. D'Aguanno, M. A. Vincenti, M. Scalora, and M. J. Bloemer, Phys. Rev. B **85**, 205430 (2012).

[29]H. Shen, and B. Maes, Appl. Phys. Lett. **100**, 241104 (2012).

[30]R. H. Fan, L. H. Zhu, R. W. Peng, X. R. Huang, D. X. Qi, X. P. Ren, Q. Hu, and Mu Wang, Phys. Rev. B **87**, 195444 (2013).

[31]R. W. Wood, Philos. Mag. **4**, 396 (1902).

[32]R. W. Wood, Phys. Rev. **48**, 928 (1935).

[33]J. T. Shen, P. B. Catrysse, and S. Fan, Phys. Rev. Lett. **94**, 197401 (2005).

[34]G. Subramania, S. Foteinopoulou, and I. Brener, Phys. Rev. Lett. **107**, 163902 (2011).

[35]J. D. Edmunds, M. J. Lockyear, A. P. Hibbins, J. R. Sambles, and I. J. Youngs, Appl. Phys. Lett. **102**, 011120 (2013).

[36]P. Yeh, Opt. Commun. **26**, 289 (1978).

[37]H. A. Atwater, and A. Polman, Nat. Mater. **9**, 205 (2010).

[38]A. Taflove, and S. C. Hagness, *Computational Electrodynamics: The Finite-Difference*

Time-Domain Method, *3rd ed*. (Artech House, Norwood, MA, 2005).

[39]X. R. Huang, and R. W. Peng, J. Opt. Soc. Am. A **27**, 718 (2010).

[40]H. E. Went, A. P. Hibbins, J. R. Sambles, C. R. Lawrence, and A. P. Crick, Appl. Phys. Lett. **77**, 2789 (2000).

[41]S. Collin, G. Vincent, R. Haïdar, N. Bardou, S. Rommeluère, and J. L. Pelouard, Phys. Rev. Lett. **104**, 027401 (2010).

[42]P. H. Siegel, IEEE Trans. Microwave Theory Tech. **50**, 910 (2002).

[43]B. Ferguson, and X. C. Zhang, Nat. Mater. **1**, 26 (2002).

[44]M. Tonouchi, Nat. Photon. **1**, 97 (2007).

[45]E. Hendry, M. J. Lockyear, J. Gómez Rivas, L. Kuipers, and M. Bonn, Phys. Rev. B **75**, 235305 (2007).

[46]M. Shalaby, H. Merbold, M. Peccianti, L. Razzari, G. Sharma, T. Ozaki, R. Morandotti, T. Feurer, A. Weber, L. Heyderman, B. Patterson, and H. Sigg, Appl. Phys. Lett. **99**, 041110 (2011).

[47]X. J. Liu, J. Q. Gu, R. Singh, Y. F. Ma, J. Zhu, Z. Tian, M. X. He, J. G. Han, and W. L. Zhang, Appl. Phys. Lett. **100**, 131101 (2012).

Figures:

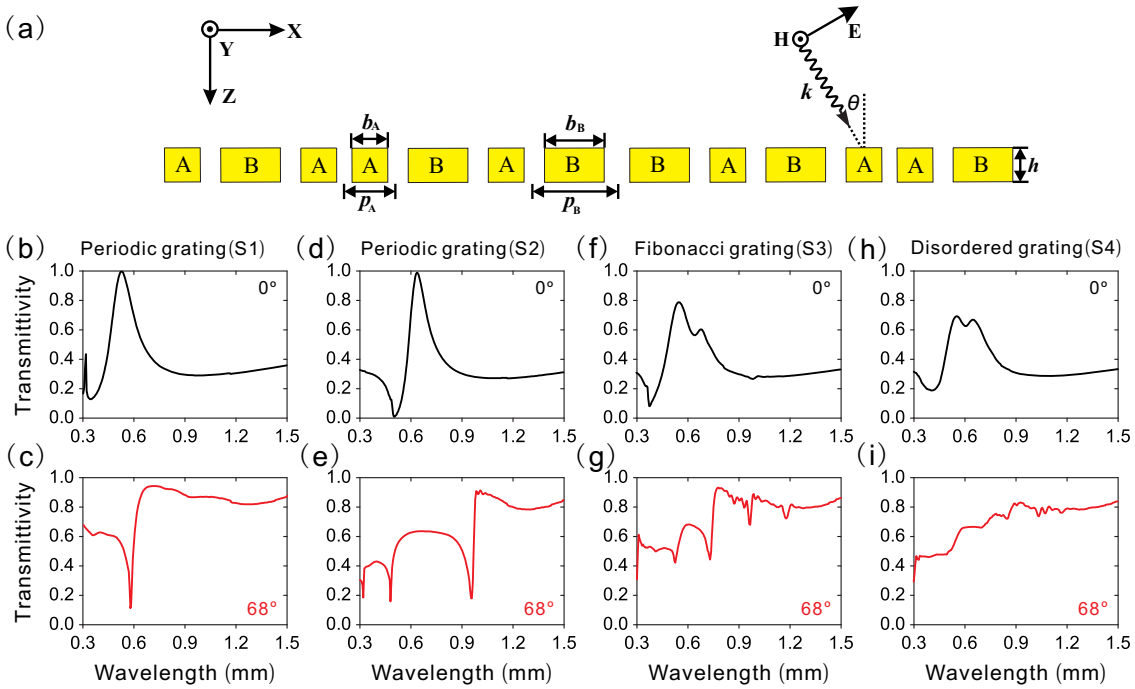

FIG. 1. (Color online). **(a)** Schematic of metallic grating with non-periodic sequence (Fibonacci sequence, disordered sequence, etc.) constructed by units *A* and *B*. Calculated transmission spectra for TM polarization of structures: a periodic metallic grating (S1) constructed by unit *A* when incident angle **(b)** $\theta = 0°$ and **(c)** $\theta = 68°$; a periodic metallic grating (S2) constructed by unit *B* when incident angle **(d)** $\theta = 0°$ and **(e)** $\theta = 68°$; a metallic grating with the tenth-generation Fibonacci sequence (S3) constructed by units *A* and *B* when incident angle **(f)** $\theta = 0°$ and **(g)** $\theta = 68°$; a metallic grating with disordered sequence (S4) constructed by units *A* and *B* when incident angle **(h)** $\theta = 0°$ and **(i)** $\theta = 68°$. Unit sizes of units *A* and *B* are $p_A = 300\ \mu$m and $p_B = 500\ \mu$m, strip widths of units *A* and *B* are $b_A = 210\ \mu$m and $b_B = 350\ \mu$m, the thickness of all gratings are $h = 200\ \mu$m.

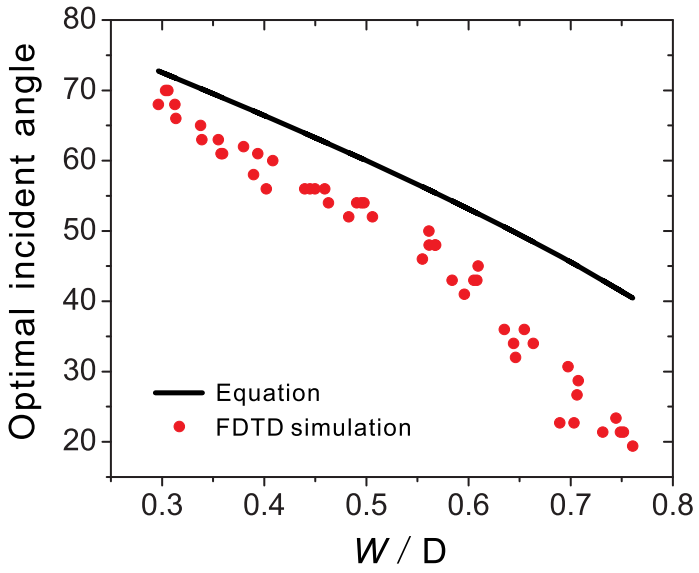

FIG. 2. (Color online). Dependence of the optimal incident angle on the average air void filling ratio W / D obtained by θ_f = arcos (W / D) (black line) and FDTD simulation (red dot). In the simulation, the width of all slits and strips are generated randomly, but the average air void filling ratio W / D is fixed for each simulation sample. Each sample of our simulation is about 4 cm in width and contains about 100 metal strips.

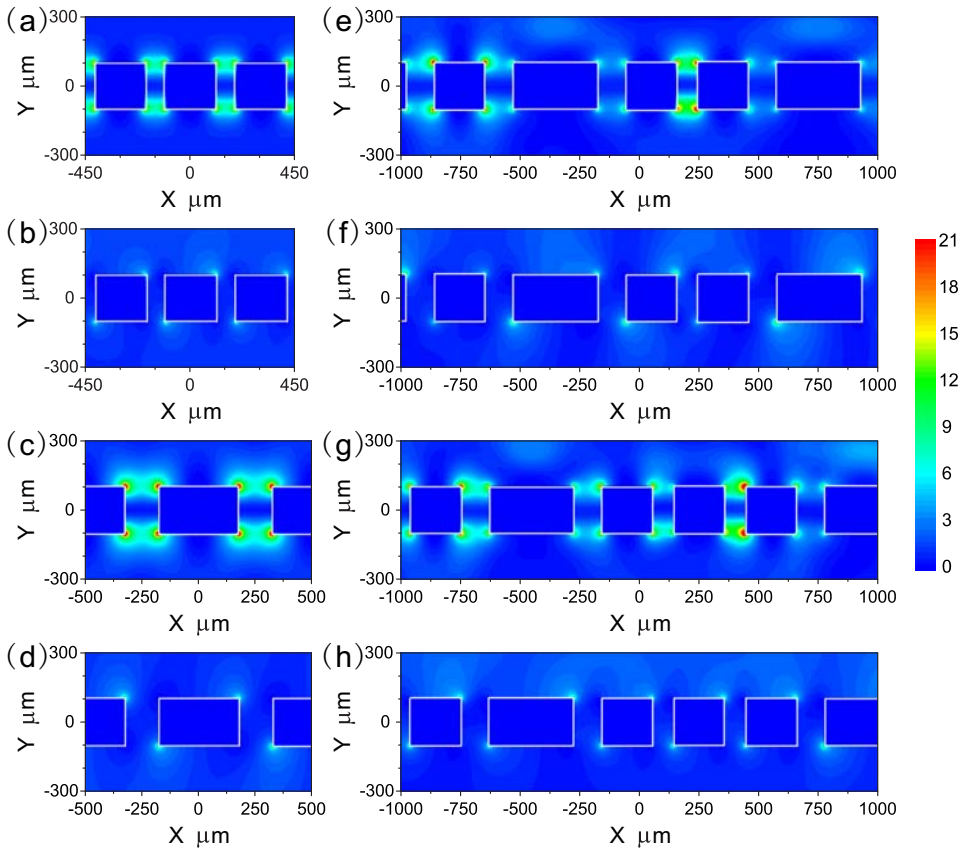

FIG. 3. (Color online). Calculated electric field ($|\mathbf{E}|^2$) distributions of a periodic metallic grating constructed by unit *A*: **(a)** $\theta = 0°$ at $\lambda = 525$ μm; **(b)** $\theta = 68°$ at $\lambda = 1200$ μm. Calculated $|\mathbf{E}|^2$ distributions of a periodic metallic grating constructed by unit *B*: **(c)** $\theta = 0°$ at $\lambda = 635$ μm; **(d)** $\theta = 68°$ at $\lambda = 1200$ μm. Calculated $|\mathbf{E}|^2$ distributions of a metallic grating with the tenth-generation Fibonacci sequence constructed by units *A* and *B*: **(e)** $\theta = 0°$ at $\lambda = 550$ μm; **(f)** $\theta = 68°$ at $\lambda = 1200$ μm. Calculated $|\mathbf{E}|^2$ distributions of a metallic grating with disordered sequence constructed by units *A* and *B*: **(g)** $\theta = 0°$ at $\lambda = 550$ μm; **(h)** $\theta = 68°$ at $\lambda = 1200$ μm. Unit sizes of units *A* and *B* are $p_A = 300$ μm and $p_B = 500$ μm, strip widths of units *A* and *B* are $b_A = 210$ μm and $b_B = 350$ μm, the thickness of all gratings are $h = 200$ μm.

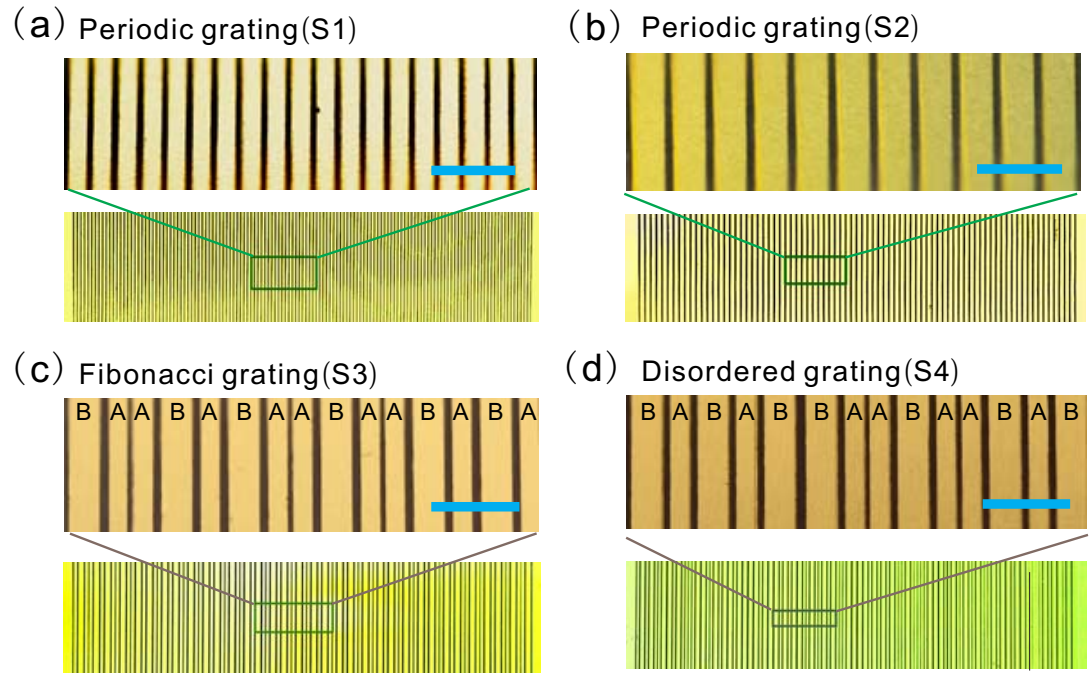

FIG. 4. (Color online). **(a)** Photograph of periodic metallic grating (S1) constructed by unit *A*. **(b)** Photograph of periodic metallic grating (S2) constructed by unit *B*. **(c)** Photograph of a metallic grating with the tenth-generation Fibonacci sequence (S3) constructed by units *A* and *B*. **(d)** Photograph of a metallic grating with disordered sequence (S4) constructed by units *A* and *B*. The scale bar is 1 mm for all the four photographs. Unit sizes of units *A* and *B* are p_A = 300 μm and p_B = 500 μm, strip widths of units *A* and *B* are b_A = 210 μm and b_B = 350 μm, the thickness of all gratings are h = 200 μm.

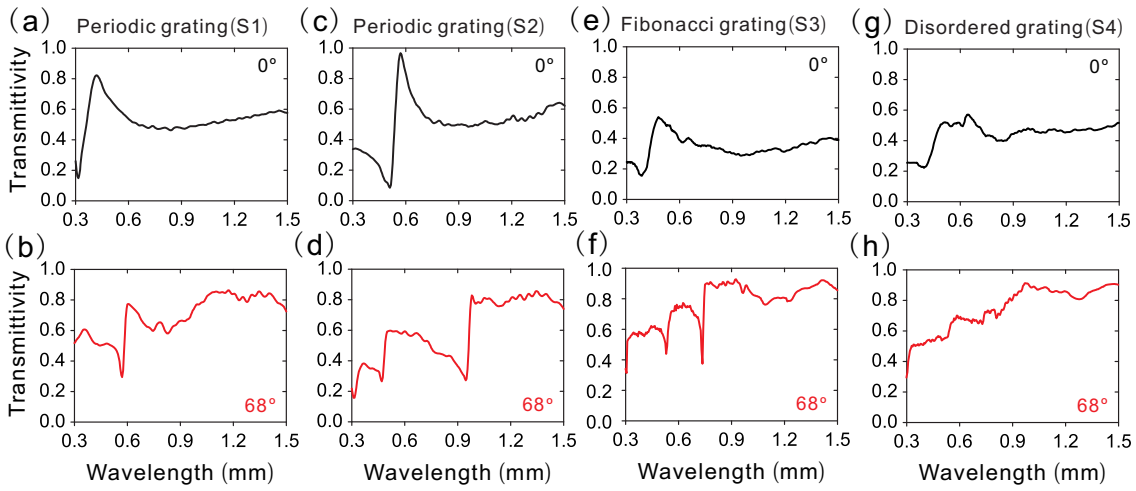

FIG. 5. (Color online). Experimentally measured transmission spectra of a periodic metallic grating (S1) constructed by unit *A* when incident angle **(a)** θ = 0° and **(b)** θ = 68°. Experimentally measured transmission spectra of a periodic metallic grating (S2) constructed by unit *B* when incident angle **(c)** θ = 0° and **(d)** θ = 68°. Experimentally measured transmission spectra of a metallic grating with the tenth-generation Fibonacci sequence (S3) constructed by units *A* and *B* when incident angle **(e)** θ = 0° and **(f)** θ = 68°. Experimentally measured transmission spectra of a metallic grating with disordered sequence (S4) constructed by units *A* and *B* when incident angle **(g)** θ = 0° and **(h)** θ = 68°. Experimentally measured transmission spectra are carried out at incident angle θ = 0° and θ = 68° for TM polarization. Unit sizes of units *A* and *B* are p_A = 300 μm and p_B = 500 μm, strip widths of units *A* and *B* are b_A = 210 μm and b_B = 350 μm, the thickness of all gratings are h = 200 μm.

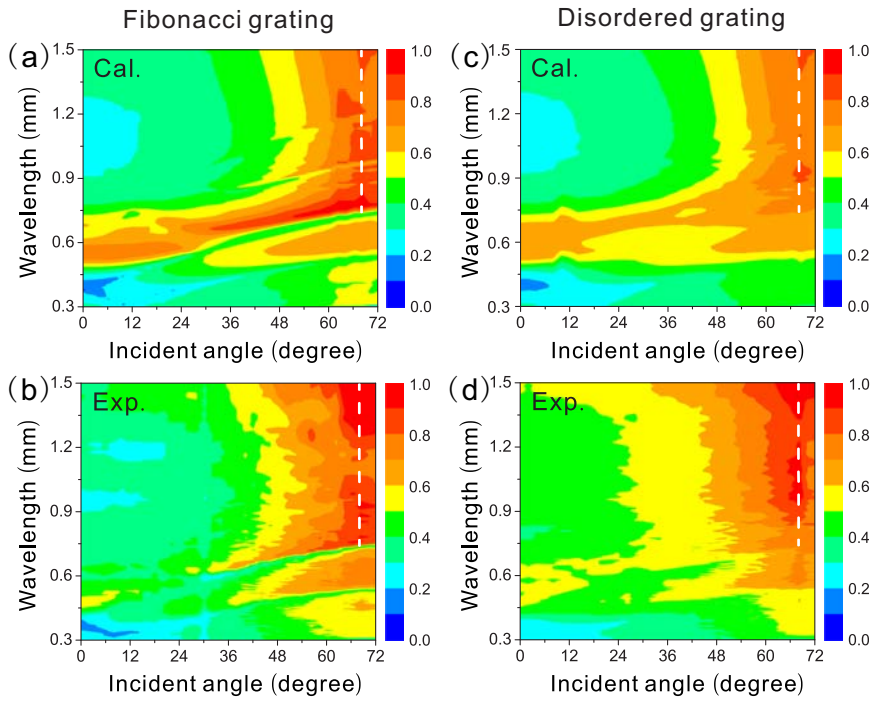

FIG. 6. (Color online). **(a)** Calculated and **(b)** experimentally measured angular transmission spectra for a metallic grating with the tenth-generation Fibonacci sequence constructed by units *A* and *B* for TM polarization. **(c)** Calculated and **(d)** experimentally measured angular transmission spectra for a metallic grating with disordered sequence constructed by units *A* and *B* for TM polarization. The color bars show the transmission intensity. The white dashed lines represent the incident angle with maximum transmission. Unit sizes of units *A* and *B* are p_A = 300 μm and p_B = 500 μm, strip widths of units *A* and *B* are b_A = 210 μm and b_B = 350 μm, the thickness of all gratings are h = 200 μm.

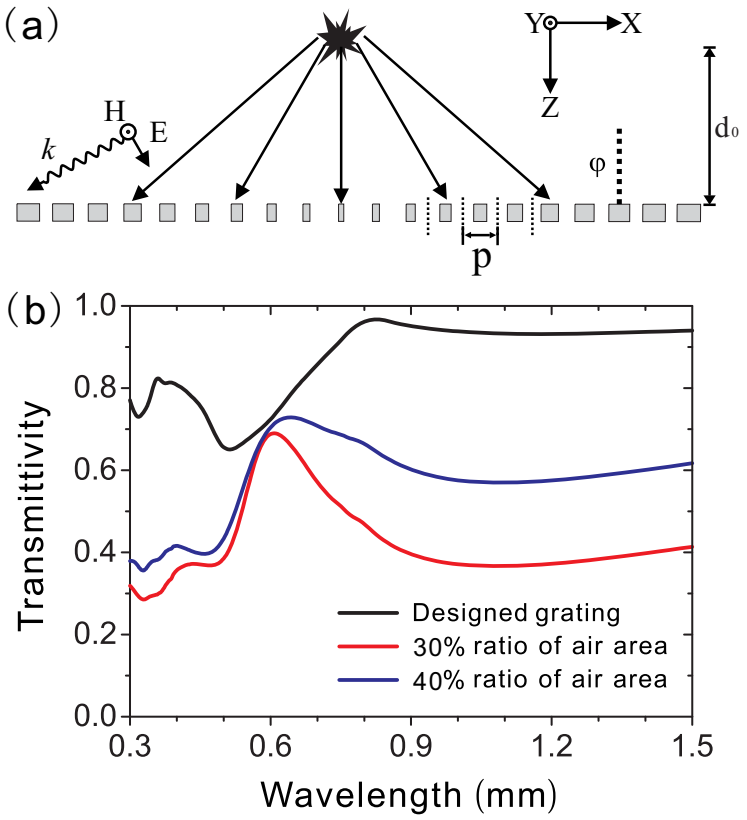

FIG. 7. (Color online). **(a)** Schematic of the specially designed grating for the TM polarized line source. The structure consists of units along the X-axis, which have a length of p = 0.4 mm and a thickness of h = 200 μm. The distance between the line source and sample is d_0 = 2 mm. The air void filling ratio of each unit is decided according to the incident angle φ. **(b)** Calculated transmission spectra for different metallic gratings for the TM polarized line source. The black line is the transmission spectra of the specially designed grating for the TM polarized line source. The red line and blue line show the periodic grating with 30% and 40% air void filling ratio, respectively.